

# How reproducible are surface areas calculated from the BET equation?

Johannes W. M. Osterrieth<sup>a</sup>, James Rampersad<sup>a</sup>, David Madden<sup>a</sup>, Nakul Rampal<sup>a</sup>, Luka Skoric<sup>b</sup>, Bethany Connolly<sup>a</sup>, Mark D. Allendorf<sup>c</sup>, Vitalie Stavila<sup>c</sup>, Jonathan L. Snider<sup>c</sup>, Rob Ameloot<sup>d</sup>, João Marreiros<sup>d</sup>, Conchi Ania<sup>e</sup>, Diana Azevedo<sup>f</sup>, Enrique Vilarrasa-Garcia<sup>f</sup>, Bianca F. Santos<sup>f</sup>, Xian-He Bu<sup>g</sup>, Ze Chang<sup>g</sup>, Hana Bunzen<sup>h</sup>, Neil R. Champness<sup>i</sup>, Sarah L. Griffin<sup>i</sup>, Banglin Chen<sup>j</sup>, Rui-Biao Lin<sup>j</sup>, Benoit Coasne<sup>k</sup>, Seth Cohen<sup>l</sup>, Jessica C. Moreton<sup>l</sup>, Yamil J. Colon<sup>m</sup>, Linjiang Chen<sup>n</sup>, Rob Clowes<sup>n</sup>, François-Xavier Couderc<sup>o</sup>, Yong Cu<sup>p</sup>, Bang Hou<sup>p</sup>, Deanna M. D'Alessandro<sup>q</sup>, Patrick W. Doherty<sup>q</sup>, Mircea Dincă<sup>r</sup>, Chenyue Sun<sup>r</sup>, Christian Doonan<sup>s</sup>, Michael Thomas Huxley<sup>s</sup>, Jack D. Evans<sup>t</sup>, Paolo Falcaro<sup>u</sup>, Raffaele Ricco<sup>u</sup>, Omar Farha<sup>v</sup>, Karam B. Idrees<sup>v</sup>, Timur Islamoglu<sup>v</sup>, Pingyun Feng<sup>w</sup>, Huajun Yang<sup>w</sup>, Ross S. Forgan<sup>x</sup>, Dominic Bara<sup>x</sup>, Shuhei Furukawa<sup>y</sup>, Eli Sanchez<sup>y</sup>, Jorge Gascon<sup>z</sup>, Selvedin Telalovic<sup>z</sup>, Sujit K. Ghosh<sup>aa</sup>, Soumya Mukherjee<sup>aa</sup>, Matthew R. Hill<sup>ab</sup>, Muhammed Munir Sadiq<sup>ab</sup>, Patricia Horcajada<sup>ac</sup>, Pablo Salcedo-Abraira<sup>ac</sup>, Katsumi Kaneko<sup>ad</sup>, Radovan Kukobat<sup>ad</sup>, Jeff Kenvin<sup>ae</sup>, Seda Keskin<sup>af</sup>, Susumu Kitagawa<sup>ag</sup>, Ken-ichi Otake<sup>ag</sup>, Ryan P. Lively<sup>ah</sup>, Stephen J. A. DeWitt<sup>ah</sup>, Phillip Llewellyn<sup>aj</sup>, Bettina V. Lotsch<sup>aj,ak</sup>, Sebastian T. Emmerling<sup>aj,ak</sup>, Alexander M. Pütz<sup>aj,ak</sup>, Carlos Martí-Gastaldo<sup>al</sup>, Natalia Padial<sup>al</sup>, Javier García-Martínez<sup>am</sup>, Noemi Linares<sup>am</sup>, Daniel MasPOCH<sup>an,ao</sup>, Jose A. Suárez del Pino<sup>ao</sup>, Peyman Moghadam<sup>ap</sup>, Rama Oktavian<sup>ap</sup>, Russel E. Morris<sup>aq</sup>, Paul S. Wheatley<sup>aq</sup>, Jorge Navarro<sup>ar</sup>, Camille Petit<sup>as</sup>, David Danaci<sup>as</sup>, Matthew J. Rosseinsky<sup>at</sup>, Alexandros P. Katsoulidis<sup>at</sup>, Martin Schröder<sup>au</sup>, Xue Han<sup>au</sup>, Sihai Yang<sup>au</sup>, Christian Serre<sup>av</sup>, Georges Mouchaham<sup>av</sup>, David S. Sholl<sup>ah</sup>, Raghuram Thyagarajan<sup>ah</sup>, Daniel Siderius<sup>aw,aw</sup>, Randall Q. Snurr<sup>ax</sup>, Rebecca B. Goncalves<sup>ay</sup>, Shane Telfer<sup>az</sup>, Seok J. Lee<sup>az</sup>, Valeska P. Ting<sup>ba</sup>, Jemma L. Rowlandson<sup>ba</sup>, Takashi Uemura<sup>bb</sup>, Tomoya Iiyuka<sup>bb</sup>, Monique A. van der Veer<sup>bc</sup>, Davide Rega<sup>bc</sup>, Veronique Van Speybroeck<sup>bd</sup>, Sven M. J. Rogge<sup>bd</sup>, Aran Lemaire<sup>bd</sup>, Krista S. Walton<sup>ah</sup>, Lukas W. Binge<sup>ah</sup>, Stefan Wuttke<sup>be,bf</sup>, Jacopo Andreato<sup>be,bf</sup>, Omar Yaghi<sup>bg,bh</sup>, Bing Zhang<sup>bg</sup>, Cafer T. Yavuz<sup>bi</sup>, Thien S. Nguyen<sup>bi</sup>, Felix Zamora<sup>bj</sup>, Carmen Montoro<sup>bj</sup>, Hongcai Zhou<sup>bk</sup>, Angelo Kirchner<sup>bk</sup>, and David Fairen-Jimenez<sup>a,\*</sup>

<sup>a</sup> The Adsorption & Advanced Materials Laboratory (A<sup>2</sup>ML), Department of Chemical Engineering & Biotechnology, University of Cambridge, Philippa Fawcett Drive, Cambridge CB3 0AS, UK

<sup>b</sup> Cavendish Laboratory, University of Cambridge, JJ Thomson Avenue, CB3 0HE, Cambridge, United Kingdom

<sup>c</sup> Sandia National Laboratories, 7011 East Avenue, Livermore, California 94550, United States

<sup>d</sup> cMACS, Department of Microbial and Molecular Systems (M<sup>2</sup>S), KU Leuven, 3001 Leuven, Belgium

<sup>e</sup> CEMHTI, CNRS (UPR 3079), Université d'Orléans, 45071 Orléans, France

<sup>f</sup> LPAC02/GPSA, Department of Chemical Engineering, Federal University of Ceará, 60455-760 Fortaleza (CE), Brazil

<sup>g</sup> School of Materials Science and Engineering, National Institute for Advanced Materials, Nankai University, Tianjin 300350, China

<sup>h</sup> Chair of Solid State and Materials Chemistry, Institute of Physics, University of Augsburg, Universitaetsstrasse 1, Augsburg 86159, Germany

<sup>i</sup> School of Chemistry, University of Nottingham, University Park, Nottingham, NG7 2RD UK

40 <sup>j</sup> Department of Chemistry, University of Texas at San Antonio, One UTSA Circle, San Antonio, TX 78249-  
 41 0698, USA

42 <sup>k</sup> Univ. Grenoble Alpes, CNRS, LIPhy, 38000 Grenoble, France

43 <sup>l</sup> Department of Chemistry and Biochemistry, University of California, San Diego, La Jolla, California, 92093  
 44 USA

45 <sup>m</sup> Department of Chemical and Biomolecular Engineering, University of Notre Dame, Notre Dame, IN, 46556,  
 46 USA

47 <sup>n</sup> Leverhulme Research Centre for Functional Materials Design, Materials Innovation Factory and  
 48 Department of Chemistry, University of Liverpool, Liverpool, UK

49 <sup>o</sup> Chimie ParisTech, PSL University, CNRS, Institut de Recherche de Chimie Paris, 75005 Paris, France

50 <sup>p</sup> School of Chemistry and Chemical Engineering, Shanghai Jiaotong University, 800 Dongchuan Road,  
 51 Minhang District, Shanghai

52 <sup>q</sup> School of Chemistry, The University of Sydney, New South Wales, 2006, Australia

53 <sup>r</sup> Department of Chemistry, Massachusetts Institute of Technology, Cambridge, Massachusetts 02139, USA

54 <sup>s</sup> Centre for Advanced Nanomaterials and Department of Chemistry, The University of Adelaide, North  
 55 Terrace, Adelaide, SA 5000, Australia

56 <sup>t</sup> Department of Inorganic Chemistry, Technische Universität Dresden, Bergstrasse 66, 01062, Dresden,  
 57 Germany

58 <sup>u</sup> Institute of Physical and Theoretical Chemistry, Graz University of Technology, Graz, Austria

59 <sup>v</sup> Department of Chemistry and International Institute of Nanotechnology, Northwestern University, 2145  
 60 Sheridan Road, Evanston, Illinois 60208, United States

61 <sup>w</sup> Department of Chemistry, University of California, Riverside, California 92521, USA

62 <sup>x</sup> WestCHEM School of Chemistry, University of Glasgow, Glasgow, UK

63 <sup>y</sup> Institute for Integrated Cell-Material Sciences, Kyoto University, Yoshida, Sakyo-ku, Kyoto 606-8501, Japan

64 <sup>z</sup> KAUST Catalysis Center (KCC), King Abdullah University of Science and Technology, P.O.Box 4700,  
 65 23955-6900, Thuwal-Jeddah, Kingdom of Saudi Arabia

66 <sup>aa</sup> Department of Chemistry, Indian Institute of Science Education and Research (IISER), Pune, Dr. Homi  
 67 Bhabha Road, Pashan, Pune 411008, India

68 <sup>ab</sup> CSIRO, Private Bag 33, Clayton South MDC, VIC 3169, Australia and Department of Chemical  
 69 Engineering, Monash University, Clayton, VIC 3168, Australia

70 <sup>ac</sup> Advanced Porous Materials Unit (APMU), IMDEA Energy, Avda. Ramón de la Sagra 3, E-28935 Móstoles,  
 71 Madrid, Spain

72 <sup>ad</sup> Research Initiative for Supra-Materials, Shinshu University, Nagano, Japan

73 <sup>ae</sup> Micromeritics Instrument Corporation, Norcross, GA 30093, USA

74 <sup>af</sup> Department of Chemical and Biological Engineering, Koc University, Rumelifeneri Yolu 34450 Sariyer,  
 75 Istanbul, Turkey

76 <sup>ag</sup> Institute for Integrated Cell-Material Sciences (WPI-iCeMS), Kyoto University Institute for Advanced Study  
 77 (KUIAS), Kyoto University, Yoshida Ushinomiya-cho, Sakyo-ku, Kyoto 606-8501, Japan

78 <sup>ah</sup> School of Chemical & Biomolecular Engineering, Georgia Institute of Technology, Atlanta, GA 30332, USA

79 <sup>ai</sup> CNRS / Aix-Marseille Univ. / TOTAL

80 <sup>aj</sup> Max Planck Institute for Solid State Research, Heisenbergstrasse 1, 70569 Stuttgart, Germany

81 <sup>ak</sup> Department of Chemistry, University of Munich (LMU), Butenandtstrasse 5-13, 81377 Munich, Germany

82 <sup>al</sup> Instituto de Ciencia Molecular (ICMol), Universitat de València, Paterna 46980, València, Spain

83 <sup>am</sup> Laboratorio de Nanotecnología Molecular, Departamento de Química Inorgánica, Universidad de Alicante,  
 84 Ctra. San Vicente-Alicante s/n, E-03690 San Vicente del Raspeig, Spain

85 <sup>an</sup> ICREA, Pg. Lluís Companys 23, Barcelona, 08010, Spain  
 86 <sup>ao</sup> Catalan Institute of Nanoscience and Nanotechnology (ICN2), CSIC and the Barcelona Institute of Science  
 87 and Technology. Campus UAB, Bellaterra, 08193 Barcelona, Spain  
 88 <sup>ap</sup> Department of Chemical and Biological Engineering, The University of Sheffield, United Kingdom  
 89 <sup>aq</sup> School of Chemistry, University of St Andrews, North Haugh, St Andrews, KY16 9ST, UK  
 90 <sup>ar</sup> Departamento de Química Inorgánica, Universidad de Granada, 18071 Granada, Spain  
 91 <sup>as</sup> Barrer Centre, Department of Chemical Engineering, Imperial College London, London, U.K., SW7 2AZ  
 92 <sup>at</sup> Materials Innovation Factory, Department of Chemistry, University of Liverpool, Liverpool, L7 3NY, UK  
 93 <sup>au</sup> School of Chemistry, The University of Manchester, Manchester, U.K. M13 9PL  
 94 <sup>av</sup> Institut des Matériaux Poreux de Paris, Ecole Normale Supérieure, ESPCI Paris, CNRS, PSL University,  
 95 75005 Paris, France  
 96 <sup>aw</sup> Chemical Sciences Division, National Institute of Standards and Technology, Gaithersburg, Maryland USA  
 97 20899-8320  
 98 <sup>ax</sup> Departments of Chemical & Biological Engineering, Northwestern University, 2145 Sheridan Road,  
 99 Evanston, Illinois 60208, USA  
 100 <sup>ay</sup> Department of Chemistry, Northwestern University, 2145 Sheridan Road, Evanston, Illinois 60208, USA  
 101 <sup>az</sup> MacDiarmid Institute for Advanced Materials and Nanotechnology, Institute of Fundamental Sciences,  
 102 Massey University, Palmerston North, 4442 New Zealand  
 103 <sup>ba</sup> Department of Mechanical Engineering, University of Bristol, Bristol BS8 1TR, U.K.  
 104 <sup>bb</sup> Department of Advanced Materials Science, Graduate School of Frontier Sciences, The University of  
 105 Tokyo, 5-1-5 Kashiwanoha, Kashiwa, Chiba 277-8561, Japan  
 106 <sup>bc</sup> Department of Chemical Engineering, Delft University of Technology, van der Maasweg 9, 2629HZ Delft,  
 107 the Netherlands  
 108 <sup>bd</sup> Center for Molecular Modeling (CMM), Ghent University, Technologiepark 46, B-9052 Zwijnaarde, Belgium  
 109 <sup>be</sup> BCMaterials, Basque Center for Materials, Applications and Nanostructures, UPV/EHU Science Park,  
 110 48940, Leioa, Spain  
 111 <sup>bf</sup> IKERBASQUE, Basque Foundation for Science, 48009, Bilbao, Spain  
 112 <sup>bg</sup> Department of Chemistry, University of California—Berkeley; Kavli Energy Nanoscience Institute at UC  
 113 Berkeley  
 114 <sup>bh</sup> Berkeley Global Science Institute, Berkeley, California 94720, United States  
 115 <sup>bi</sup> Department of Chemical and Biomolecular Engineering, Korea Advanced Institute of Science and  
 116 Technology (KAIST), Yuseong-gu, 34141 Daejeon, Korea  
 117 <sup>bj</sup> Departamento de Química Inorgánica, Universidad Autónoma de Madrid, 28049 Madrid, Spain  
 118 <sup>bk</sup> Chemistry Department -Texas A&M University  
 119 <sup>ψ</sup> Official contribution of the National Institute of Standards and Technology (NIST), not subject to copyright in  
 120 the United States of America  
 121 <sup>φ</sup> Certain commercially available items may be identified in this paper. This identification does not imply  
 122 recommendation by NIST, nor does it imply that it is the best available for the purposes described  
 123 \* E-mail: [df334@cam.ac.uk](mailto:df334@cam.ac.uk)

124 Porosity and surface area analysis play a prominent role in modern materials science, where  
125 their determination spans the fields of natural sciences, engineering, geology and medical  
126 research. At the heart of this sits the Brunauer-Emmett-Teller (BET) theory,<sup>[1]</sup> which has been  
127 a remarkably successful contribution to the field of materials science. The BET method was  
128 developed in the 1930s for open surfaces but is now the most widely used metric for the  
129 estimation of surface areas of micro- and mesoporous materials.<sup>[2]</sup> Since the BET method  
130 was first developed, there has been an explosion in the field of nanoporous materials with  
131 the discovery of synthetic zeolites,<sup>[3]</sup> nanostructured silicas,<sup>[4–6]</sup> metal-organic frameworks  
132 (MOFs),<sup>[7]</sup> and others. Despite its widespread use, the manual calculation of BET surface  
133 areas causes a significant spread in reported areas, resulting in reproducibility problems in  
134 both academia and industry. To prove this, we have brought together 60 labs with strong  
135 track records on the study of nanoporous materials. We provided eighteen *already measured*  
136 raw adsorption isotherms and asked these researchers to calculate the corresponding BET  
137 areas. This round-robin exercise resulted in a wide range of values for each isotherm. We  
138 demonstrate here that the reproducibility of BET area determination from identical isotherms  
139 is a largely ignored issue, raising critical concerns over the reliability of reported BET areas  
140 in micro- and mesoporous materials in the literature. To solve this major issue, we have  
141 developed a new computational approach to accurately and systematically determine the  
142 BET area of nanoporous materials. Our software, called BET Surface Identification (BETSI),  
143 expands on the well-known Rouquerol criteria and makes, for the first time, an unambiguous  
144 BET area assignment possible.

145 The Brunauer-Emmett-Teller (BET) equation is arguably one of the most used equations in physical  
146 chemistry and porosimetry. Since its conception in the 1930s<sup>[1]</sup> to estimate open surfaces whilst  
147 working with non-microporous adsorbents of the time such as Fe/Cu catalysts, silica gel and  
148 charcoal, it found widespread use in the characterisation of synthetic zeolites.<sup>[3]</sup> Furthermore, it has  
149 gained considerable momentum following the discovery of more complex porous materials such as  
150 mesoporous silicas<sup>[4–6]</sup>, porous coordination polymers (PCPs)<sup>[8]</sup>, metal-organic frameworks (MOFs)<sup>[7]</sup>  
151 and covalent organic frameworks (COFs)<sup>[9]</sup>. Novel porous materials are of significant academic and  
152 industrial interest due to their applications in gas storage and separation,<sup>[10–13]</sup> catalysis,<sup>[14]</sup>  
153 sensing,<sup>[15,16]</sup> and drug delivery.<sup>[17]</sup> To assess their adsorptive properties, Langmuir was the first to  
154 relate gas adsorption isotherms to surface areas, assuming only monolayer adsorption.<sup>[18]</sup> This was  
155 in contrast to Dubinin's proposition of micropore volumes for microporous materials.<sup>[19]</sup> Langmuir's  
156 adsorption theory was later extended to multilayer adsorption, resulting in the titular BET model.  
157 Even though the BET theory was not developed for describing adsorption in the microporosity, the  
158 BET area is now the *de facto* standard for the characterisation of any porous material. Indeed, it has  
159 been recognized by the International Union of Pure and Applied Chemistry (IUPAC) as "the most  
160 widely used procedure for evaluating the surface area of porous and finely-divided materials".<sup>[2,20]</sup>  
161 Furthermore, it has been an International Organization for Standardization (ISO) standard for surface

162 area determination since 1995.<sup>[21]</sup> This makes it, arguably, the most important figure of merit for  
163 porous materials, including microporous ones. Looking at the literature, it is clear that the idea of  
164 monolayer coverage or even the concept of surface area are necessarily idealised and therefore  
165 could be inaccurate descriptions for microporous materials.<sup>[22]</sup> Indeed, IUPAC warns users to apply  
166 “extreme caution [when using the BET equation] in the presence of micropores. (...) [The BET area]  
167 represents an *apparent* surface area, which may be regarded as a useful adsorbent ‘fingerprint’.”<sup>[2]</sup>  
168 This more nuanced understanding of the BET area is mirrored in the writing of Rouquerol *et al.*, “the  
169 meaning of the BET surface is (...) that it embraces the major part of the amount of adsorptive in  
170 energetic interaction with the surface.”<sup>[22]</sup> Despite these cautionary words, the BET area remains a  
171 deeply engrained metric in the fields of physical chemistry and materials science. Given the broad  
172 use of the BET equation, it is not surprising to see that much has been written on the *applicability*  
173 and the *accuracy* of the BET theory – that is, its model of the adsorption process – and on the  
174 reproducibility of the raw data, *i.e.* the adsorption isotherm.<sup>[23–26]</sup>

175 Since the development of the first porous materials, there has been a sharp rise in the design  
176 of highly ordered and structured porous materials (**Fig. S1**).<sup>[27,28]</sup> The advent of materials with more  
177 complex pore networks and dynamic frameworks through material design strategies such as reticular  
178 chemistry has given rise to reported BET areas in excess of 8,000 m<sup>2</sup> g<sup>-1</sup>.<sup>[11,29–34]</sup> Often, these modern  
179 materials have complex adsorption isotherms which are more problematic or ambiguous to fit to the  
180 BET model, *e.g.* several steps can occur due to different pore types and/or flexibility being present  
181 in the material.<sup>[35]</sup> In response, a new generation of porosimetry equipment with pressure transducers  
182 capable of recording high-resolution gas adsorption isotherms at ultra-low pressures (<10<sup>-5</sup> mmHg)  
183 has been developed. However, reliance on manual calculations of surface areas using the BET  
184 method remains commonplace. In this context, ‘manual’ refers to the judicious selection of a  
185 pressure range by a scientist, be it through a self-developed spreadsheet or commercial software.  
186 This raises the question of the *reproducibility* of BET calculations *from the same isotherm*. An  
187 adsorption isotherm with 150 points has more than 10,000 consecutive combinations of points, all  
188 of which are potentially correct fitting ranges and will return different BET areas. The answer to the  
189 question of which is the optimal fitting region is far from obvious, and the consequence of any  
190 irreproducibility or different interpretations are serious. Consider two groups synthesizing the same  
191 compound and reporting two different BET areas; Sample A is reported to have a BET area of 1,500  
192 m<sup>2</sup> g<sup>-1</sup> and Sample B’s reported BET area is 2,000 m<sup>2</sup> g<sup>-1</sup>. Unless there is a common standard and  
193 protocol for calculating BET areas, we cannot say for certain that the quality and adsorption  
194 performance of Sample A is lower than that of Sample B. Indeed, the lack of reproducibility of MOF  
195 syntheses and adsorption performance, by comparing reported BET areas, has been highlighted  
196 already, but the natural spread of BET calculations was not included in the analysis.<sup>[36]</sup>

197 The eponymously named Rouquerol criteria (**Section S2**, Supplementary Information) aim to  
198 ensure good practice in identifying a valid fitting range, and, as such, they have found widespread  
199 acceptance in the literature and have been adopted in both IUPAC and ISO standards.<sup>[2,20–22,24,25,37]</sup>

200 Despite this safeguard, we herein propose that current BET area calculations are irreproducible for  
201 two reasons: first, the Rouquerol criteria are indeterminate in identifying the correct fitting region, as  
202 they apply to multiple regions simultaneously. Second, even if they were determinate, they are too  
203 cumbersome and lengthy to implement and are therefore often neglected in practice. This dilemma  
204 is reminiscent of the Skeptic's Argument from Gorgias, here paraphrased: i) the BET area does not  
205 exist (e.g., for microporous materials); ii) even if it exists, it cannot be systematically and  
206 unequivocally calculated (i.e., determined by the Rouquerol criteria).

207 To prove our hypothesis and to assess the current spread of BET calculation results, we have  
208 shared a dataset of 18 isotherms (reported as relative pressure vs. amount adsorbed), already  
209 measured, and representing four classes of micro- and mesoporous materials (zeolites, mesoporous  
210 silicas, MOFs and COFs) with 60 laboratories with expertise in adsorption science and synthesis of  
211 porous materials. In this round-robin exercise, we asked the researchers to calculate the BET areas  
212 in the way they saw most fit. More details about the specific materials and the adsorption isotherms,  
213 sampled both from our laboratory and from the NIST/ARPA-E database,<sup>[38]</sup> are included in the  
214 Supplementary Information, **Section S10**. To avoid any recognition bias, all isotherms were  
215 anonymised and scaled-off arbitrarily. **Figure 1a** shows the large spread of results obtained from  
216 manual calculations of BET areas in the round-robin experiment, the full details can be found  
217 anonymised in the Supplementary Information, tabulated in **Section S3**, and represented graphically  
218 in **Section S4**. Most groups (90%) reported using the Rouquerol criteria in their manual calculation,  
219 23% used a commercial software package, and 6% used a self-developed code. Details on the  
220 methods for each group can be found in **Section S11** of the Supporting Information. Bar a few  
221 exceptions, virtually no two groups of experts reported identical BET areas for any given isotherm.  
222 We observed a spread of at least 300 m<sup>2</sup> g<sup>-1</sup> for each isotherm; however, that number was  
223 significantly higher for some individual isotherms. For NU-1104, a modern MOF with substantial  
224 porosity (isotherm **Figure 1b**),<sup>[32]</sup> the highest estimate of 9,341 m<sup>2</sup> g<sup>-1</sup> and the lowest estimate of  
225 1,757 m<sup>2</sup> g<sup>-1</sup> differed by an astonishing 7,584 m<sup>2</sup> g<sup>-1</sup>, making the highest estimate more than five  
226 times higher than the lowest estimate. The spread of values for frequently reproduced MOFs such  
227 as HKUST-1, MOF-5 and ZIF-8 was slightly smaller than that of literature cited values.<sup>[36]</sup> While this  
228 observation affirms the natural assumption that material synthesis and isotherm measurement play  
229 a more important role in determining the BET area than the calculation, we can nevertheless attribute  
230 a significant portion of this spread to current BET fittings. The results of this social study demonstrate  
231 that there is significant variation in BET area calculations from the same isotherm, as it is extremely  
232 unlikely for two researchers to select identical fitting regions. At this point, we propose a novel  
233 method that not only systematically selects an optimal fitting region but does so by eliminating all  
234 other hypothetical fitting regions. With thousands of consecutive combinations of points, the large  
235 number of potential fittings is impossible to carry out manually.

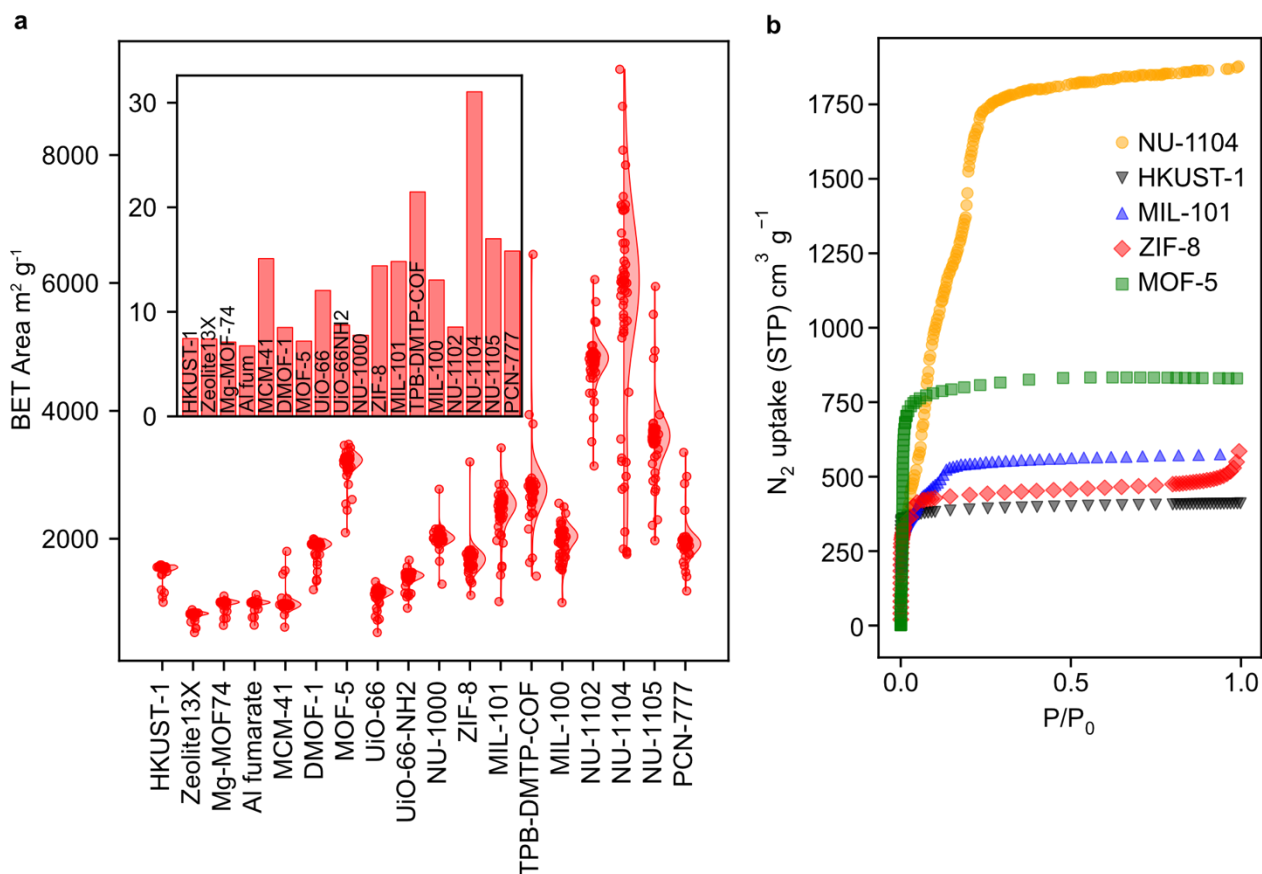


**Figure 1 | Round-robin results of BET area calculation.** **a**, Distribution of BET areas from identical isotherms as calculated by 60 laboratories with an expertise in adsorption science and synthesis of porous materials. Superimposed are normalised probability distribution functions obtained by kernel density estimation. Inset shows the coefficient of variation (relative standard deviation) of results for each material **b**, Exemplary isotherms for materials shown in **a**. The large spread of BET areas reported for NU-1104 is due to the unusual shape of its adsorption isotherm, making manual BET fits difficult.

To solve the problem of manual BET fitting, we developed a computational tool for BET analysis, *BET Surface Identification* (BETSI). This tool makes an unambiguous calculation of the BET area based on the original Rouquerol criteria but modified to prevent manual interaction, requiring only the adsorption isotherm as input data. As such, the results obtained from the round-robin evaluation were compared with the BETSI calculations to assess the inter-rater reliability of manual BET calculations. **Figure 2** shows the working principle of the BETSI algorithm on a simplified N<sub>2</sub> adsorption isotherm at 77 K for ZIF-8 (full details can be found in the Supporting Information, **Section S5**). First, the linearized BET equation is fitted to a particular region of the isotherm using an ordinary least-squares (OLS) regression (**Figure 2a**). The top panel shows the isotherm with a fitting region highlighted in red, and the OLS regression is shown below. The plot insets show the checks against the Rouquerol criteria (**Figure 2b**). If all criteria are met, the fitting is passed. This calculation is looped over all data intervals of at least 10 points on the isotherm. The resulting BET fits are stored in a large  $n \times n$  matrix, where the  $(j,i)$ -matrix element corresponds to a fitting region starting at the  $j^{\text{th}}$ -point and ending on the  $i^{\text{th}}$ -point (**Figure 2c**). All valid fitting results are output and plotted against the percentage error under the 4<sup>th</sup> Rouquerol criterion (**Figure 2d**). Alongside, BETSI outputs all

other BET parameters, such as monolayer capacity and the C constant, as well as full regression diagnostics (Section S5).

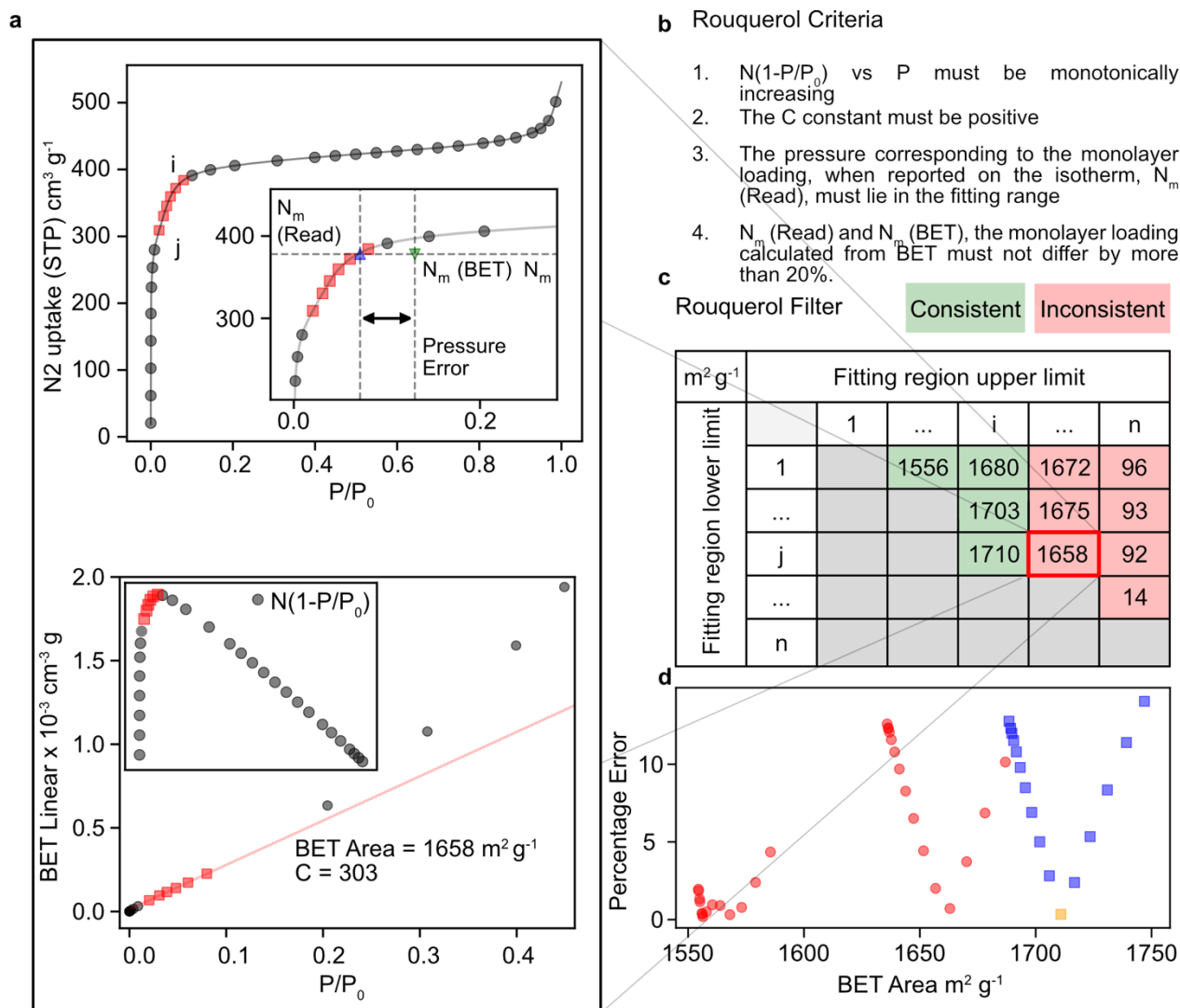


**Figure 2 | Working principle for BETSI algorithm.** **a**, The isotherm is shown with a particular fitting region highlighted in red. The linear BET equation is applied, and an ordinary least squares regression is applied to the fitting region. **b**, Subsequent checks against the Rouquerol criteria<sup>[24]</sup> are performed (insets) and **c**, valid fits are passed, The analysis shown in **a** is repeated for all consecutive combinations of points on the isotherm. A results matrix with  $n \times n$  dimensionality stores all acceptable and rejected fits **d**, All acceptable BET areas are output and plotted against the percentage error under the 4<sup>th</sup> Rouquerol criterion. (**a**, top inset). All BET areas ending on the highest permissible point under the 1<sup>st</sup> Rouquerol criterion (**a**, bottom inset, maximum in  $N(1-P/P_0)$  function) are labelled as the isotherm knee and shown in blue. The BETSI Optimal BET area (yellow) belongs to the isotherm knee group and has the lowest percentage error under the 4<sup>th</sup> Rouquerol criterion.

Since multiple fittings comply with the Rouquerol criteria (**Figure 2c-d**), BETSI demonstrates that an unambiguous assignment of the BET area is impossible under the Rouquerol criteria alone. This proves our hypothesis that the criteria in their current form are indeterminate. For the prototypical ZIF-8 isotherm, a flexible MOF with narrow windows,<sup>[35]</sup> valid BET areas fall within a range of 1,550 and 1,750  $m^2 g^{-1}$  (**Figure 2c-d**). BETSI assigns special relevance to fitting ranges that end on the highest permissible point, which are usually dictated by the 1<sup>st</sup> Rouquerol criterion, and labels these as the isotherm knee. Beyond the isotherm knee, adsorptive activity decreases

277 rapidly as the pores are mostly filled and the internal surfaces are saturated. Within this subset of  
278 BET areas, the BETSI optimum is chosen as the one with the smallest percentage error under the  
279 4<sup>th</sup> Rouquerol criterion, thus making the BET assignment unambiguous.

280 Next, we ran BETSI on the isotherms distributed in the round-robin experiment. In all cases, the  
281 spread of potential BETSI results (*i.e.*, those in agreement with the Rouquerol criteria) was  
282 considerably narrower than that obtained by manual calculation (**Table 1**). **Figure 3a** shows the  
283 individual results from the social experiment and the comparison with the BETSI results; the  
284 corresponding variation coefficients are shown in **Section S6** and an alternative representation  
285 normalised to the BETSI range is shown in **Section S7**. Since most groups reported using the  
286 Rouquerol criteria to calculate their BET areas, this substantiates our second hypothesis – that the  
287 manual implementation of the Rouquerol criteria is cumbersome and difficult to carry out in practice.  
288 For instance, in the case of NU-1104, the range of estimates decreases from 7,500 m<sup>2</sup> g<sup>-1</sup> in the  
289 social study to 235 m<sup>2</sup> g<sup>-1</sup> under BETSI. Interestingly, some isotherms gave much larger spreads of  
290 results than others, suggesting that the BET model does not describe them as naturally and thus  
291 they are more susceptible to problems associated with the Rouquerol criteria. Unsurprisingly, we  
292 also observed this trend in the round-robin evaluation. To further investigate the goodness of the  
293 isotherm fittings, we define the *BETSI variation coefficient* as the relative standard deviation of BETSI  
294 results, and the *pass rate* as the number of BET fits that pass under the Rouquerol criteria as a  
295 fraction of all potential fits. Further, the *Hit Rate* expresses the fractional number of BET areas  
296 calculated in the round-robin exercise that lie within the BETSI range. **Figure 3b** demonstrates the  
297 correlation between the *pass rate*, the *BETSI variation coefficient*, and the *Hit Rate*. Simply put, the  
298 more BET fits are valid, the greater the spread of possible BET areas is, and the more likely  
299 researchers are to satisfy the Rouquerol criteria in manual calculations. To account for the non-equal  
300 spacing of points on all different isotherms, the *pressure-adjusted pass rate* expresses the total sum  
301 of pressure intervals that fit Rouquerol criteria as a fraction of the sum of all pressure intervals of the  
302 hypothetical fitting ranges (**Section S8**). From **Figure 3b**, we classify adsorption isotherms into three  
303 broad categories, types A, B and C (**Figure 3c**). While it is difficult to generalise about the shape of  
304 these isotherms, we still offer some discussion of common features. Type A isotherms fit the BET  
305 model 'best'. Under BETSI, they have a relatively high pass rate and return a fairly narrow spread of  
306 results. Examples include materials such as Al-fumarate, NU-1000, Zeolite-13X and MCM-41. Many  
307 of these isotherms do not have strongly pronounced isotherm knees and some have mesoporous  
308 steps. Hit rates greater than 70% are generally observed for these materials, suggesting that the  
309 majority of researchers did not struggle with the fittings. Type B isotherms only fit the BET model  
310 over a very limited range. These have extremely low pass rates, meaning that only few BET fits are  
311 valid, which in turn will be spread narrowly. Examples include MOF-5, DMOF-1, NU-1104, HKUST-  
312 1, and NU-1105. For the latter, out of 9,409 hypothetical 10-point fits, only one is permissible under  
313 the Rouquerol criteria. Such prohibitively low pass rates make the correct BET assignment by hand  
314 virtually impossible and demonstrate the need for computational support. In contrast to type A

isotherms, type B isotherms often have sharp isotherm knees following strong adsorptive interactions at low relative pressures. Isotherms with more complex shapes such as NU-1104 also appear in this category. Type C isotherm fittings are arguably the most problematic. They have high pass rates and, concomitantly, they return large spreads of BET results. Typical materials that fit into this category are MIL-101, MIL-100, TPB-DMTP-COF and PCN-777. Like type A isotherms, these have rounded isotherm knees, which appear at higher relative pressures. It is for these materials that the necessity to extend the Rouquerol criteria is demonstrated and the BETSI algorithm makes an unambiguous BET assignment possible.

**Table 1 | Results of BETSI analysis and round-robin evaluation for the isotherms used in the study.** *Material*, isotherm of material under investigation; *BETSI*, optimal BET area predicted by BETSI; *BETSI Range*, full spread of BET areas that pass under BETSI; *BETSI Variation Coefficient*, relative standard deviation of BET areas that pass under BETSI; *Pass Rate*, number of BET areas that pass under BETSI expressed as a fraction of all hypothetical fittings; *Round-robin Average*, mean of BET areas calculated in round-robin evaluation; *Round-robin Range*, full spread of BET areas determined in round-robin evaluation; *Round-robin Variation Coefficient*, relative standard deviation of BET areas calculated in round-robin evaluation; *Hit Rate*, fraction of BET areas calculated in the round-robin evaluation that lie within the BETSI range.

Material	BETSI $\text{m}^2 \text{g}^{-1}$	BETSI Range $\text{m}^2 \text{g}^{-1}$	BETSI Variation Coefficient %	Pass Rate %	Round- robin Average $\text{m}^2 \text{g}^{-1}$	Round- robin Range $\text{m}^2 \text{g}^{-1}$	Round- robin Variation Coefficient %	Hit Rate %
HKUST-1	1556	8	0.090	2.419	1520	583	7.451	52
Zeolite13X	833	4	0.140	0.538	813	356	7.405	35
Mg-MOF74	1010	5	0.114	2.300	990	459	7.101	48
Al-Fumarate	1007	14	0.398	1.736	989	478	6.740	60
MCM-41	1001	60	1.573	3.329	994	1186	15.090	85
DMOF-1	1924	4	0.074	0.107	1860	795	8.500	15
MOF-5	3255	20	0.250	0.071	3170	1382	7.203	13
UiO-66	1145	91	1.901	0.870	1120	796	12.045	65
UiO-66-NH <sub>2</sub>	1424	285	4.710	1.722	1388	750	8.727	48
NU-1000	2068	160	1.619	4.218	2014	1486	7.752	80
ZIF-8	1709	188	3.718	0.861	1672	2085	14.396	58
MIL-101	2446	680	8.353	3.738	2429	2404	14.816	78
TPB-DMTP- COF	2875	711	7.298	5.375	2787	5031	21.472	80
MIL-100	2199	616	7.611	12.111	1964	1554	13.042	78
NU-1102	4931	204	1.139	0.862	4770	2915	8.541	38
NU-1104	5684	235	1.327	0.024	5553	7584	31.047	5
NU-1105	3635	0	0.000	0.011	3585	3974	16.991	0
PCN-777	2079	483	5.624	6.960	1946	2168	15.814	87

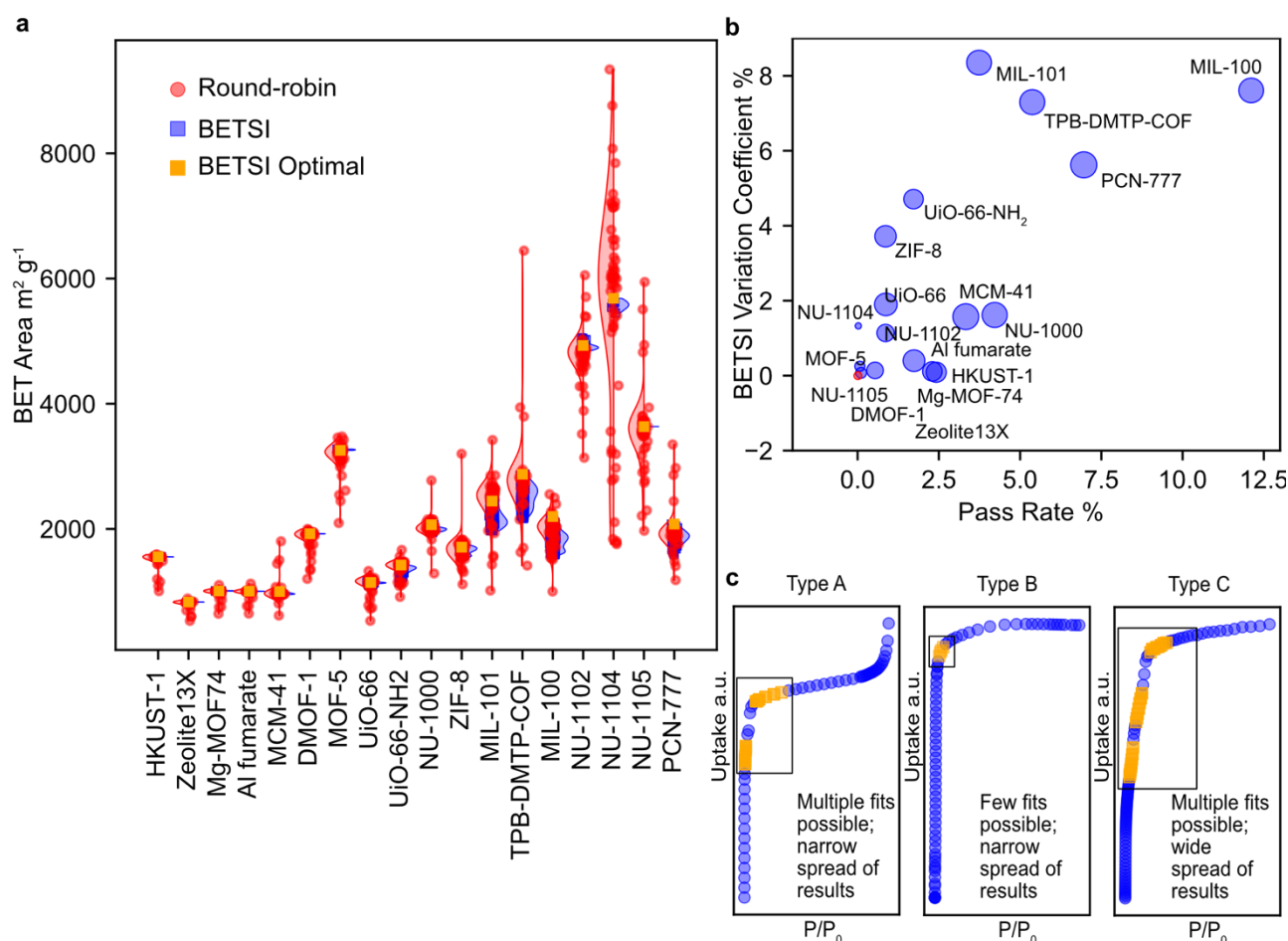


**Figure 3 | Social study results vs BETSI results.** **a**, Distribution of BET areas for identical isotherms from the social study (red) and BETSI (blue). Superimposed is the BETSI optimum (yellow). Note that the distributions of values obtained by BETSI are considerably narrower in all cases than those in the social study **b**, Plot of the BETSI Variation Coefficient (relative standard deviation of BETSI results) against the pass rate (fraction of valid fits against all hypothetical ones). Bubble size scales with the hit rate, the fraction of results from the social study that lie within the BETSI range. Red symbols have a hit rate of zero. Note the positive correlation between all three parameters **c**, Isotherm fit classifications. Type A fits have a relatively wide fitting window, within which multiple fits are possible, but return a relatively narrow spread of BET results. Type B fits have a narrow fitting window and concomitantly return a narrow set of spread of results. Type C fits have wide fitting windows, which translates to multiple passable fits and a wide spread of permissible BET areas.

## Outlook

BET theory is a great success story. Developed in the 1930s for non-microporous, open surfaces, it continues to this day to be applied to modern adsorbents with complex porosity. Despite the advances from classical density functional theory (DFT) methods, the BET area will likely continue playing a crucial role in porosimetry for decades to come, with impacts in energy research, transport, medical applications and climate-change mitigation. In light of these future developments, it will become increasingly important to share critical scientific metrics reliably to find a common language to report both academic and industrial progress.

Here, we have demonstrated the difficulties in unambiguously determining BET areas from adsorption isotherms, which in turn affect the assessment of material quality and reproducibility. These problems arise from imperfect and insufficient manual calculations and can only be met using

355 modern computational methods. Furthermore, we propose BETSI as a step towards greater  
356 transparency and criticality in determining BET areas. We stress here that it is neither the function  
357 nor the purpose of BETSI to eliminate doubt and treat a particular BET area as 'true'. Researchers  
358 should remain aware of the limitations of BET theory when applied to microporous adsorbents in  
359 general and when BET areas are reported, the pressure range and number of points used should  
360 always be stated. We further recommend here that isotherms must be reported transparently and in  
361 detail, *i.e.* semi-log representation to show the low-pressure regions. The 'experiment' is the  
362 adsorption isotherm – not the BET area.

363

## 364 Online Content

365 Source and extended data, details of author contributions and detailed instructions about the use of  
366 BETSI are included in the supplementary information.

367 Isotherm data reported with this paper are included in the NIST/ARPA-E Database of Novel and  
368 Emerging Adsorbent Materials, <https://adsorption.nist.gov>, and may be accessed directly at  
369 <https://adsorption.nist.gov/isodb/index.php?DOI=10.XXXX/YYYYY#biblio>.

370

## 371 References

- 372 [1] S. Brunauer, P. H. Emmett, E. Teller, *J. Am. Chem. Soc.* **1938**, *60*, 309–319.  
373 [2] M. Thommes, K. Kaneko, A. V. Neimark, J. P. Olivier, F. Rodriguez-Reinoso, J. Rouquerol, K. S. W.  
374 Sing, *Pure Appl. Chem.* **2015**, *87*, 1051–1069.  
375 [3] R. Cid, R. Arriagada, F. Orellana, *J. Catal.* **1983**, *80*, 228–230.  
376 [4] D. Zhao, J. Feng, Q. Huo, N. Melosh, G. H. Fredrickson, B. F. Chmelka, G. D. Stucky, *Science* **1998**,  
377 *279*, 548–552.  
378 [5] J. S. Beck, J. C. Vartuli, W. J. Roth, M. E. Leonowicz, C. T. Kresge, K. D. Schmitt, C. T. W. Chu, D.  
379 H. Olson, E. W. Sheppard, S. B. McCullen, et al., *J. Am. Chem. Soc.* **1992**, *114*, 10834–10843.  
380 [6] A. Corma, *Chem. Rev.* **1997**, *97*, 2373–2419.  
381 [7] H. C. Zhou, J. R. Long, O. M. Yaghi, *Chem. Rev.* **2012**, *112*, 673–674.  
382 [8] S. Kitagawa, R. Kitaura, S. I. Noro, *Angew. Chemie - Int. Ed.* **2004**, *43*, 2334–2375.  
383 [9] C. S. Diercks, O. M. Yaghi, *Science* **2017**, *355*, DOI 10.1126/science.aal1585.  
384 [10] J. Li, J. Sculley, H. Zhou, *Chem. Rev.* **2012**, *112*, 869–932.  
385 [11] O. K. Farha, A. Ö. Yazaydin, I. Eryazici, C. D. Malliakas, B. G. Hauser, M. G. Kanatzidis, S. T.  
386 Nguyen, R. Q. Snurr, J. T. Hupp, *Nat. Chem.* **2010**, *2*, 944–948.  
387 [12] B. Li, H.-M. Wen, W. Zhou, B. Chen, *J. Phys. Chem. Lett.* **2014**, *5*, 3468–3479.  
388 [13] P. Z. Moghadam, T. Islamoglu, S. Goswami, J. Exley, M. Fantham, C. F. Kaminski, R. Q. Snurr, O. K.  
389 Farha, D. Fairen-Jimenez, *Nat. Commun.* **2018**, *9*, 1378–1385.  
390 [14] A. Corma, H. García, F. X. Llabrés i Xamena, *Chem. Rev.* **2010**, *110*, 4606–4655.  
391 [15] L. E. Kreno, K. Leong, O. K. Farha, M. Allendorf, R. P. Van Duyne, J. T. Hupp, *Chem. Rev.* **2012**,  
392 *112*, 1105–1125.

- [16] W. P. Lustig, S. Mukherjee, N. D. Rudd, A. V. Desai, J. Li, S. K. Ghosh, *Chem. Soc. Rev.* **2017**, *46*, 3242–3285.
- [17] P. Horcajada, R. Gref, T. Baati, P. K. Allan, G. Maurin, P. Couvreur, G. Férey, R. E. Morris, C. Serre, *Chem. Rev.* **2012**, *112*, 1232–1268.
- [18] I. Langmuir, *J. Am. Chem. Soc.* **1918**, *40*, 1361–1403.
- [19] Y. K. Tovbin, *Russ. Chem. Bull.* **1998**, *47*, 637–643.
- [20] K. S. W. Sing, D. H. Everett, R. A. W. Haul, L. Moscou, R. A. Pierotti, J. Rouquerol, T. Siemieniewska, *Pure Appl. Chem.* **1985**, DOI 10.1351/pac198557040603.
- [21] ISO [International Organization for Standardization], *Ref. number ISO* **2010**, DOI 10.1007/s11367-011-0297-3.
- [22] J. Rouquerol, F. Rouquerol, P. Llewellyn, G. Maurin, K. S. W. Sing, *Adsorption by Powders and Porous Solids: Principles, Methodology and Applications: Second Edition*, **2013**.
- [23] F. Ambroz, T. J. Macdonald, V. Martis, I. P. Parkin, *Small Methods* **2018**, *2*, 1800173.
- [24] D. A. Gómez-Gualdrón, P. Z. Moghadam, J. T. Hupp, O. K. Farha, R. Q. Snurr, *J. Am. Chem. Soc.* **2016**, *138*, 215–24.
- [25] K. S. Walton, R. Q. Snurr, *J. Am. Chem. Soc.* **2007**, *129*, 8552–8556.
- [26] J. Park, J. D. Howe, D. S. Sholl, *Chem. Mater.* **2017**, *29*, 10487–10495.
- [27] P. Z. Moghadam, A. Li, S. B. Wiggins, A. Tao, A. G. P. Maloney, P. A. Wood, S. C. Ward, D. Fairen-Jimenez, *Chem. Mater.* **2017**, *29*, 2618–2625.
- [28] M. E. Davis, *Nature* **2002**, *417*, 813–821.
- [29] H. Furukawa, K. E. Cordova, M. O’Keeffe, O. M. Yaghi, *Science* **2013**, *341*, 1230444–1230444.
- [30] O. M. Yaghi, *J. Am. Chem. Soc.* **2016**, *138*, 15507–15509.
- [31] O. K. Farha, I. Eryazici, N. C. Jeong, B. G. Hauser, C. E. Wilmer, A. A. Sarjeant, R. Q. Snurr, S. T. Nguyen, A. Ö. Yazaydin, J. T. Hupp, *J. Am. Chem. Soc.* **2012**, *134*, 15016–15021.
- [32] T. C. Wang, W. Bury, D. A. Gómez-Gualdrón, N. A. Vermeulen, J. E. Mondloch, P. Deria, K. Zhang, P. Z. Moghadam, A. A. Sarjeant, R. Q. Snurr, et al., *J. Am. Chem. Soc.* **2015**, *137*, 3585–3591.
- [33] Z. Chen, P. Li, R. Anderson, X. Wang, X. Zhang, L. Robison, L. R. Redfern, S. Moribe, T. Islamoglu, D. A. Gómez-Gualdrón, et al., *Science* **2020**, *368*, 297–303.
- [34] I. M. Hönicke, I. Senkovska, V. Bon, I. A. Baburin, N. Bönisch, S. Raschke, J. D. Evans, S. Kaskel, *Angew. Chemie - Int. Ed.* **2018**, *57*, 13780–13783.
- [35] D. Fairen-Jimenez, S. A. Moggach, M. T. Wharmby, P. A. Wright, S. Parsons, T. Düren, *J. Am. Chem. Soc.* **2011**, *133*, 8900–8902.
- [36] M. Agrawal, R. Han, D. Herath, D. S. Sholl, *Proc. Natl. Acad. Sci. U. S. A.* **2020**, *117*, 877–882.
- [37] J. Rouquerol, P. Llewellyn, F. Rouquerol, *Stud. Surf. Sci. Catal.* **2007**, *160*, 49–56.
- [38] D.W. Siderius, V.K. Shen, R.D. Johnson III, and R.d. van Zee, Eds., NIST/ARPA-E Database of Novel and Emerging Adsorbent Materials, National Institute of Standards and Technology, Gaithersburg MD, 20899, <https://dx.doi.org/10.18434/T43882>, (retrieved August 10, 2020).

## 434 **Methods**

### 435 **Round-robin evaluation**

436 N<sub>2</sub> adsorption isotherms of 18 different materials (Supplementary Information **Section S10**) were  
437 sent to international collaborators: HKUST-1, ZIF-8, NU-1000, MIL-101, UiO-66, Al fumarate,  
438 Zeolite13X, Mg-MOF-74, UiO-66-NH<sub>2</sub>, MOF-5, DMOF-1, MCM-41, TPB-DMTP-COF, MIL-100, NU-  
439 1102, NU-1104, NU-1105, and PCN-777; they were anonymised and labelled A-R respectively. Note  
440 that this is not the order in which the isotherms appear in the paper. The isotherms were sampled  
441 from our own group measurements and from the NIST Adsorption Database. Arbitrary scaling factors  
442 were introduced to minimise recollection bias of the isotherms. The isotherms were sent out in .csv  
443 format. All colleagues received the same email with the same set of instructions (**Section S9**): To  
444 calculate the BET area from the data in the way they saw most fit and to report a rough estimate of  
445 how long it took them to calculate them. An anonymised one-page summary of each lab's own  
446 account of their calculation can be found in the Supporting Information, **Section S11**.

447 For easier data handling, once rescaled, all results were rounded to the next integer. None of  
448 the data points has been eliminated. The data is presented as a jitter plot for each material, with a  
449 superimposed kernel-density estimation obtained in python.

### 450 **BETSI**

451 The BETSI algorithm, including executables, is fully published in the Electronic Supplementary  
452 Information (<https://github.com/fairen-group/betsi-gui>). The programme is written in python and uses  
453 principally the numpy library. Looped linear regressions over all consecutive combinations of at least  
454 three points, perform full BET analyses and store the fitting parameters in n x n results matrices,  
455 where the (j,i)-matrix element denotes a linear regression from the j'th to the i'th point on the  
456 isotherm. Binary pass/fail matrices with the same dimensionality are used independently to assess  
457 compliance with linearity and fitting criteria. The 'filtering' of BET areas is achieved by element-wise  
458 matrix multiplication of the results matrices and the pass/fail matrices. This allows independent  
459 'activation' and 'deactivation' of the criteria and observing the effects on the results. The minimum  
460 fitting requirement of ten points is coded in a pass/fail matrix to allow for some minimum point  
461 flexibility, as is the cut-off value for R<sup>2</sup> of 0.995. To avoid low-leverage non-linearity in the linear  
462 region, the first Rouquerol criterion has been extended to also require the linearised BET function to  
463 increase monotonically with P/P<sub>0</sub>, as well as N(1-P/P<sub>0</sub>). The third and fourth Rouquerol criteria are  
464 implemented through a 10,000 point Pchip interpolation of the isotherm to reconstruct the N<sub>m</sub> (Read).  
465 As the third and fourth criteria require the N<sub>m</sub> (BET) to be a real value, *i.e.* they require C to be  
466 positive, the second criterion cannot be independently deactivated from the third and the fourth. The  
467 associated logic has been written into the programme. Following the BETSI filtering by multiplication  
468 of results and pass/fail matrices, the isotherm knee is identified as the subset of BET areas whose  
469 fitting region end on the highest permissible pressure point. In most cases this will be the highest  
470 permissible point under the first Rouquerol criterion. The optimal BETSI prediction is chosen as the

471 fitting region with the lowest percentage error under the fourth criterion and belonging to the isotherm  
472 knee subset.

473 BETSI only requires the adsorption isotherm as input data and returns six plots used to validate  
474 the results: the isotherm itself, with the optimal linear region highlighted as well as the BET fit; the  
475 'Rouquerol representation' of the isotherm,  $N(1-P/P_0)$  plotted against  $P/P_0$ ; the linearised plot with  
476 the OLS regression and the regression parameters; the filtered percentage error vs BET areas plot  
477 with the isotherm knee and optimal BET area highlighted; the filtered monolayer-loadings plot  
478 showing all permissible monolayer loadings on the isotherm; and the statistical distribution of  
479 permissible BET areas with a boxplot. Additionally, BETSI returns four regression diagnostics plots  
480 which can be used to assess whether the assumptions of OLS regression have been met: The  
481 Residuals vs Fitted values plot can be used to visually inspect whether the residuals are normally  
482 distributed around the regression line, and similar information can be obtained from the QQ-plot.  
483 Finally, the Scale-Location plot can be used to assess whether the distribution of studentized  
484 residuals is homoscedastic or heteroscedastic and the Residuals vs Leverage plot can be used to  
485 identify high-leverage points that have an abnormally large influence on the regression line.

#### 486 **Comparison between round-robin evaluation and BETSI results**

487 Statistical analysis of the results was performed in python. The *BETSI variation coefficient* and the  
488 *Round-robin variation coefficient* are standard deviations relative to the average of each set. The  
489 *pass rate* for each isotherm is the number of permissible BET fits as a fraction of all consecutive  
490 combination of points. To account for non-equal spacing of the points on each isotherm, the  
491 *pressure-adjusted pass-rate* is obtained by integrating along the pressure axis and dividing the total  
492 sum of permissive pressure intervals by the sum of all consecutive pressure intervals. The *hit rate* is  
493 the fractional number of BET areas calculated in the round-robin evaluation that lie within the BETSI  
494 range.

#### 495 **Author Contributions**

496 J.W.M.O. and D.F.-J. designed the study. J.W.M.O. and D.M. collected and curated the dataset of  
497 isotherms shared among coauthors. J.W.M.O., J. R., N. R., L. S. and B. C. developed BETSI code.  
498 All coauthors calculated the BET areas from the pre-measured isotherms. J.W.M.O., D. M and D.F.-  
499 J. co-wrote the paper. All authors discussed the results and contributed to the editing of the  
500 manuscript.

#### 501 **Acknowledgements**

502 This project has received funding from the European Research Council (ERC) under the European  
503 Union's Horizon 2020 research and innovation programme (NanoMOFdeli), ERC-2016-COG  
504 726380, Innovate UK (104384) and EPSRC IAA (IAA/RG85685).

505 O.K.F. and R.Q.S. acknowledge funding from the U.S. Department of Energy (DE-FG02-  
506 08ER15967).

507 R.S.F. and D.B. acknowledge funding from the European Research Council (ERC) under the  
508 European Union's Horizon 2020 research and innovation programme (SCoTMOF), ERC-2015-StG  
509 677289.

510 Sandia National Laboratories is a multimission laboratory managed and operated by National  
511 Technology and Engineering Solutions of Sandia, LLC., a wholly owned subsidiary of Honeywell  
512 International, Inc., for the U.S. Department of Energy's National Nuclear Security Administration  
513 under contract DE-NA-0003525. The authors gratefully acknowledge funding from the U.S.  
514 Department of Energy, Office of Energy Efficiency and Renewable Energy, Hydrogen and Fuel Cell  
515 Technologies Office, through the Hydrogen Storage Materials Advanced Research Consortium  
516 (HyMARC). This paper describes objective technical results and analysis. Any subjective views or  
517 opinions that might be expressed in the paper do not necessarily represent the views of the U.S.  
518 Department of Energy or the United States Government.

519 J.D.E acknowledges the support of the Alexander von Humboldt foundation and the Center for  
520 Information Services and High Performance Computing (ZIH) at TU Dresden.

521 S.K.G. and S.M. acknowledge SERB (Project No. CRG/2019/000906), India for financial support.

522 K.K. and R.K. acknowledge Active Co. Research Grant for funding.

523 S.K. acknowledge funding from the European Research Council (ERC) under the European Union's  
524 Horizon 2020 research and innovation programme (COSMOS), ERC-2017-StG 756489.

525 N.L. and J.G.M acknowledge funding from the European Commission through the H2020-MSCA-  
526 RISE-2019 program (ZEOBIOCHEM – 872102) and the Spanish MICINN and AEI/FEDER  
527 (RTI2018-099504-B-C21). N.L. thanks the University of Alicante for funding (UATALENTO17-05).

528 ICN2 is supported by the Severo Ochoa program from the Spanish MINECO (Grant No. SEV-2017-  
529 0706)

530 S.M.J.R. and A.L wish to thank the Fund for Scientific Research Flanders (FWO), under grant nos.  
531 12T3519N and 11D2220N.

532 L.S. was supported by the EPSRC Cambridge NanoDTC EP/L015978/1

533 C.T.Y. and T.S.N. acknowledges funds from the National Research Foundation of Korea, NRF-  
534 2017M3A7B4042140 and NRF-2017M3A7B4042235

535

536

537 P.F. and H. Y. acknowledge US Department of Energy, Office of Basic Energy Sciences, Materials  
538 Sciences and Engineering Division under Award No. DE-SC0010596 (P.F.).

539 R.O would like to acknowledge funding support during his Ph.D study from Indonesian Endowment  
540 Fund for Education-LPDP with the contract No. 202002220216006